Mathematical Reconstruction of Patient-Specific Vascular Networks Based on Clinical Images and Global Optimization

JUNHONG SHEN[1,2,*], **ABDUL HANNAN FARUQI**[1,3,*], **YIFAN JIANG**[1,4,6], **AND NIMA MAFTOON**[1,5]

[1]Computational Metastasis Laboratory, Department of Systems Design Engineering, University of Waterloo, Waterloo, ON N2L 3G1, Canada
[2]Department of Mathematics, University of California at Los Angeles, Los Angeles, CA 90095, USA
[3]Department of Mechanical Engineering, Aligarh Muslim University, Aligarh 202001, India
[4]Department of Mathematics, University of Toronto, Toronto, ON M5S 1A1, Canada
[5]Centre for Bioengineering and Biotechnology, University of Waterloo, Waterloo, ON N2L 3G1, Canada
[6]Department of Statistical Science, University of Toronto, Toronto, ON M5S 1A1, Canada

Corresponding author: Nima Maftoon (nmaftoon@uwaterloo.ca)

*Junhong Shen and Abdul Hannan Faruqi contributed equally to this work.

ABSTRACT Cancer is a major cause of death worldwide and becomes particularly threatening once it begins to metastasize. During metastasis, the blood vessels serve as pathways for cancerous cell transportation and hence are crucial for understanding cancer growth. Existing medical imaging modalities can provide 3-D contrast images of the vascular tissues but with limited quality and detailedness. A much-needed tool for cancer research is thus one that can reconstruct vascular networks from low-quality clinical images. To this end, we developed a computational framework that takes 3-D medical images as input and reconstructs complete, patient-specific vascular network models using a mathematical optimization procedure. Our framework extracts major vessels from the images and uses the organ geometry to select vessel termination points. Then, it generates the remainder network based on physiological optimality principles. Using the framework, we obtained a set of network models with over 3000 terminal segments from a brain MRA scan. We analyzed the Strahler order, vessel radius, and branch length distributions of the models, which match with actual human data. We also performed fluid dynamics simulation inside the reconstructed vessels and showed that the pressure and shear stress distributions agree with existing *in vivo* measurements. The qualitative and quantitative agreements in vessel morphometry and hemodynamics demonstrate the effectiveness of the framework. Our method bridges the gap between image-based vessel models, accuracy of which is limited by the resolution of clinical images, and hypothetical models.

INDEX TERMS Global constructive optimization, patient-specific vasculature, vascular network reconstruction.

I. INTRODUCTION

In metastasis, cancer cells detach from a pre-existing primary tumor, intravasate into the bloodstream, flow through blood vessels avoiding immune protection, extravasate out of the vessels, and eventually form secondary tumors at other sites [1]. Because blood vessels are vital links in the journey of the tumor cells, delineating the vessel structures may aid the development of novel methods for cancer diagnosis and metastatic growth prediction. An imperative tool for cancer research is thus a computational framework that generates patient-specific vascular models efficiently. In this paper,

we focus on vascular network reconstruction in human brains. Many recent works have studied vessel generation in the liver, heart, and eye [2]–[5]. However, similar research on cerebral vascular networks is scarce due to the non-convex geometry of the vascular territories and the multiple blood flow inlets in the brain which complicate the network structure.

In the past few decades, several theoretical models have been developed to study vessel generation in the human body. These models provide a mathematical explanation for substructure development in a vascular system. There are three major methods to construct vessel models theoretically. The angiogenesis-based method simulates the actual growth of vasculatures by considering the biological and physiological factors involved in the process. It has been used for generating

3-D vascular networks of human livers and hearts [6], [7]. The compartment model does not characterize vessels as a single organ. Instead, it lumps vessels into a compartment and models them globally by computing the resistance of the whole compartment and identifying the pressure-volume relation [8], [9]. Self-similar models are constructed over successive orders of bifurcations based on vessel generating rules [10]–[12], which focus on the self-similar features of vessels in human organs. The overall network structure is established by fractals. Although the above methods justify the general structural properties of blood vessels, they produce homogeneous network models that do not account for individual differences. Thus, the vascular networks generated entirely from theoretical principles cannot be used for customized disease treatment.

On the other hand, image-based reconstruction methods directly build 3-D geometric models that capture the high-level structure of a patient's blood vessels from clinical images (CT, MRA, etc). These methods rely on image segmentation techniques, such as pattern recognition, model-based, and tracking-based algorithms [13]. However, the segmentation quality is limited by the resolution of the clinical images. Partial merging of two vessels, spurious segmentation at crossover points, discontinuity in vessel trees, and lack of microvasculature details are commonly found in segmented vascular networks [14]–[16]. Therefore, image-based reconstruction alone is also insufficient to provide complete and detailed 3-D vasculatures that can be further used for investigating metastasis.

In this work, we cope with the limitations of theoretical and image-based vascular models by combining the two approaches. We present a hybrid reconstruction framework that integrates medical image information with angiogenesis-based optimization to generate complete, 3-D, patient-specific vascular networks of the human brain. In particular, we use segmentation techniques to obtain a coarse structure of the brain vascular network and then search for a refined configuration with optimal network material cost (MC) and power cost (PC). While MC optimization minimizes the materials needed to form blood vessels [17], i.e., endothelial cells, plasma, white, and red blood cells, PC optimization minimizes the total power required for blood circulation. To solve the optimization problem given the patient prior, we acquire the main vessel branches and terminal segments from the images and apply global constructive optimization (GCO). The original GCO algorithm performs a multi-scale optimization to find an ideal tree structure provided with a set of terminal nodes [4]. Yet it only works for generating a single tree. However, reconstructing patient-specific models requires using all available priors, i.e., all segmented main vessels. Therefore, we extend the GCO algorithm to account for the multi-tree network generation. We demonstrate the effectiveness of the proposed framework by applying it to actual brain images and validating the generated networks using data from existing literature.

II. METHODS
In this section, we first present the theoretical contribution of this work: a novel angiogenesis-based optimization algorithm for patient-specific multi-tree vascular network generation. We will start with the assumptions needed to mathematically model the vascular networks. Then, we will introduce the original GCO algorithm and formulate our extended GCO method.

The proposed algorithm accepts a main vessel structure (represented as the coordinates and the associated radii of a set of branching points) and a brain volume (represented by a point cloud in the three-dimensional space) as input. The former is used to generate the root nodes, while the latter is used to sample the leaf nodes. Given the locations of the nodes, the algorithm outputs a complete, detailed network with newly added branching nodes such that the location and associated radii of each node is optimized to reduce a predefined cost. The optimization is accomplished through two stages: local optimization at each junction of the network, and global optimization of the entire network topology.

In practice, the inputs are obtained from clinical images, and the output can be used to generate 3-D models that can be used for modelling blood flow for diagnosis or predictive purposes. We postpone the detailed discussion of the additional steps of the reconstruction framework, e.g., image processing and segmentation algorithm, to the end of this section. The complete source code can be found at github.com/nmaftoon/VesselGen.

A. ASSUMPTIONS
Our proposed method uses the following assumptions to make reconstruction of the vascular network possible.
- For the overall structure of the vascular network, we assume that the network is constructed as a collection of trees in a predefined volume, in our case, the patient's brain. We will refer to this volume as the perfusion territory in later discussions.
- Every vascular tree begins with a root segment and ends with multiple terminal segments. The terminal points (we also refer to them as leaf nodes) provide inflow for unmodeled microvasculature. The trees are assumed to be binary (having two branches at every node) to simulate the branching pattern of real blood vessels.
- The pressure drop due to branching is negligible.
- Each blood vessel segment is assumed to be a cylinder. See Fig. 1 for the bifurcation model used in our framework.
- The blood flow is assumed to be incompressible, Newtonian, and laminar. The laminar assumption is well justified in small vessels due to the predominance of viscous effects [18]. We also assume that Murray's law holds in the vascular network with a power-law coefficient of 3 corresponding to branching in small arteries [19]. Details of the mathematical formulations are in Section II-D3.
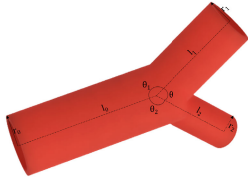
FIGURE 1. Vessel bifurcation model. A bifurcation model is uniquely defined by the locations of three end points, the location of the bifurcation point, and the radii of three incident edges. The angles between adjacent edges can be calculated using the positions of the four nodes.

- The overall vascular network satisfies the optimal physiological principles in minimizing both material and power costs [17].

| (a) Initialization | (b) Splitting |
| (c) Pruning & reconnecting | (d) Generated tree |
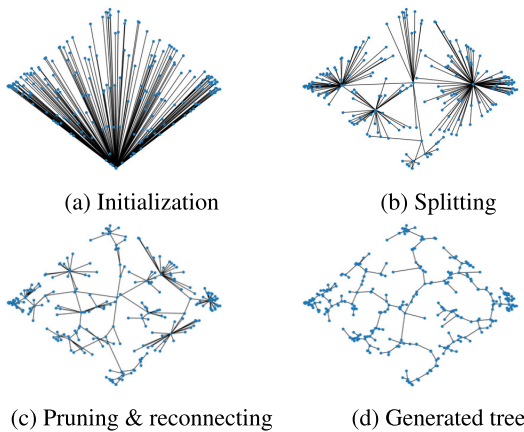
FIGURE 2. 2-D example of generating a single tree with GCO. (a) First connect all leaf nodes to the root node. The branching point locations are adjusted to minimize the cost function. (b) In splitting, a single node is split into two nodes to reduce the number of edges incident on that single node. (c) Edges with Strahler order less than a threshold are pruned. The detached nodes are connected to their nearest neighbors. (d) After optimization, the network minimizes the total loss.

B. GLOBAL CONSTRUCTIVE OPTIMIZATION (GCO)

Georg *et al.* [4] proposed the GCO algorithm to reconstruct the vascular network in the liver based on intravascular volume minimization and constraints derived from physiological optimality principles. Their algorithm takes a predefined root node and a set of leaf nodes randomly chosen from the perfused volume to reconstruct a vascular tree with one blood-flow inlet. The optimization is performed at both local and global levels. Local operators like relaxation, merging, and splitting adjust the number, radii and locations of the branching points in the vascular tree based on a predefined objective function (Fig. 2). Then, the tree is pruned so that branches with Strahler orders smaller than a threshold are removed and the leaf nodes are reconnected to the nearest neighbor to preserve only the coarse skeletal structure. Globally, the pruning threshold decreases after each round of optimization, so fewer details are pruned, resulting in a final optimized vascular tree. This algorithm can generate vascular

networks that exhibit realism in physiological properties such as branching angles and asymmetry. However, it can only be applied to organs with a single blood-flow inlet. Thus, to adapt it to the human brain, we extended the GCO algorithm to reconstruct a vasculature with multiple arteries from a segmented patient prior. Since the method requires growing several vascular trees inside the same territory, we also developed an algorithm that samples leaf nodes according to their relative positions in the brain.

C. GCO ADAPTED TO PATIENT DATA

The vascular network created by the original GCO algorithm is purely hypothetical. In that algorithm, the initial root node is manually chosen and can be adjusted. The perfusion territory does not account for any patient-specific data. Although the quantitative results on scaling and branching properties of the models, such as vessel radii and length ratios, show correspondence with real data, the gross vascular anatomy of the models are dissimilar. Therefore, the original GCO method is not suitable for reconstructing vascular networks that are meant for further medical use. In this work, we develop the GCO algorithm to work with medical images as follows.

1) ROOT NODE SELECTION

Given a patient's clinical image, we first perform 3-D segmentation to obtain the major vessel structures visible in the image. Then, we select N points from the main vessel segments as the root locations for different trees. The number of points is determined by the physiological properties of the target organ. In order to maintain the patient-specific vascular structure, every branching point and endpoint of the image segmentation result is included. The rest of the points are distributed along the vessels. To preserve as many details as possible, we add intermediate nodes between two adjacent nodes on the same vessel if their distance is larger than a threshold d, which is set to the average vessel length of the target organ in practice. Note that if there are no branches at an intermediate node, the adjacent nodes are still considered to be on the same vessel only with curvature.

2) LEAF NODE SELECTION

The leaf nodes are sampled within the inner cortical surface of the patient's brain. The brain structures through which the arteries do not penetrate, e.g., the cerebellum and the brain stem, are removed from the volume of interest. Due to the existence of multiple vascular trees, we divide the volume of interest into several perfusion territories, each with a predefined radius of influence r_{inf} that represents the size of the region that a vessel end can cover through capillary networks. If r_{inf} is large, the leaf nodes in the territory should not be too close to each other to prevent competition or overlap between vessel branches. If r_{inf} is small, we should sample more leaf nodes to cover the entire perfused volume. The radius of influence is uniquely determined for each perfusion territory and applies to all nodes within that territory. To calculate r_{inf}, we first obtain the influence score of each region, which is

the weighted average of the parameters, i.e., distances from root nodes to the center of the territory and vessel radii at the corresponding root node locations. r_{inf} is directly calculated by scaling the score using the radii range, i.e., 0.5 mm to 2.5 mm in our case [20], [21].

With r_{inf} defined for every perfusion territory, we use an iterative algorithm that samples as few as possible leaf nodes to cover the entire cortical volume. Starting with a randomly selected set of nodes, we compute the influence region of each node by its location and the corresponding r_{inf}. Then, we move the nodes that lie outside the tissue volume or overlap with existing nodes to regions that are not perfused by any of the original nodes. If necessary, new nodes are added to the uncovered areas. This process is repeated until the entire volume of interest is perfused by the selected leaf nodes.

D. GCO FOREST: EXTENSION OF GCO TO MULTIPLE TREES

We now propose an innovative method that enables the growth of several trees within the same perfusion territory using GCO. As there are N root nodes selected, the resulting vascular network can be considered as the association of N single trees. Hence we call the method GCO Forest. The details of the algorithm are described below.
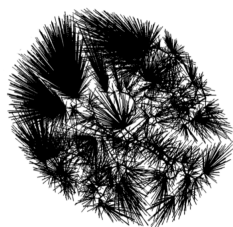
FIGURE 3. GCO Forest initialization. In the initialization step, the algorithm connects the randomly sampled leaf nodes with the nearest nodes on the segmented vessel centerline model.

1) INITIALIZATION

First, we cope with the structures extracted from the brain angiography and define the root parameters. Based on the connectivity information obtained from the clinical images, the root nodes can be linked together to form an initial vascular network (Fig. 3). Each edge in the network is modeled as a cylinder with a radius r_{root}. For every vessel tip, this radius is initialized in accordance with the patient data. It is then propagated along individual vessels before two vessels meet. For a branching point, the parent radius is derived from the daughter radii using Murray's law.

Next, we create edges that directly connect each leaf node to the nearest root node. By doing so, a subtree containing one root node and its incident leaf nodes is created and can be considered as an independent tree to apply GCO. For simplicity, the radius at each of the leaves in one subtree is initialized to a constant value. Nevertheless, we can also assign numbers derived from physiological data to the leaf radius to improve model accuracy. With the radius known for

every edge in the network, the blood flow can be calculated using the Hagen-Poiseuille's law as in [22].

2) FOREST GROWTH

The forest growth is inspired by the iterative GCO procedure used for generating a single tree. Similar to the original method, we define a cost function for each vessel segment based on the branching parameters, i.e., the vessel radius and segment length. The local cost at a bifurcation is the sum of neighboring edge costs, whereas the global cost is the sum of all edge costs in the entire network. The global costs depend both on the relative positions of the nodes in the network, as well as the global topological structure of the tree. The goal is to obtain a set of branching points (defined by their coordinates and associated radii) that minimize the global cost of the network.

Firstly, in each iteration, the branching parameters are optimized locally by **relaxation**, **splitting**, and **merging**.

- Relaxation - The location of every branching point and the radii of the incident edges is optimized at each node to minimize the local cost.
- Splitting - It takes place if the cost of creating another node is lower than that of the original configuration.
- Merging - For an intermediate node, if the ratio of the shortest incident edge to the second shortest edge is smaller than a threshold δ, we remove the shortest edge and merge the two nodes which it originally connects.

After applying several rounds of local operators, we optimize the network structure on a global scale. That is, edges with Strahler orders smaller than some threshold l_{max} are pruned and the resulting disconnected leaf nodes are reconnected to its nearest neighbor in the pruned tree. To preserve increasingly finer substructures in the network, the initial threshold l_{max} is decreased after a determinate number of iterations. However, as more nodes are added to the network due to splitting, the leaf nodes are no longer restrained to connect with the nodes from the same subtree during the reconnection process: each node can freely connect to the closest node, regardless of the subtree that the closest node belongs to. This is because, during optimization, subtrees have their preferred direction of growth, and how territories are divided should adapt to the overall branching pattern as well.

The optimization process terminates when there is no reduction in both the local and the global costs of the network. This indicates that the vascular model has reached its optimal configuration. In our method, the total number of iterations is positively related to the number of leaf nodes sampled prior to initialization. We also refer the reader to [4] for the parameter selection strategy in merging and pruning.

The GCO Forest method allows two or more trees to grow simultaneously. This is a major improvement with respect to the original GCO algorithm, which allows the reconstruction

of patient-specific vascular networks based on segmented arterial data with multiple blood-flow inlets.

3) COST FUNCTION

In this section, we illustrate the design principles of the cost function used to optimize branching point locations and the associated radii.

With fixed leaf nodes, an optimal branching point is defined by its location and neighboring edge radii that minimize the cost function. Following the work of Elif *et al.* [17], we incorporate the material cost (MC), which represents the total amount of materials required to form blood-carrying vessels, in our objective function. There are two types of materials to consider. The first one is the endothelial cells that form the vessel walls, the amount of which is proportional to the surface area of the blood vessels:

$$S = 2\pi r l, \tag{1}$$

where r and l denote the radius and the length of a vessel segment, respectively. The second types of materials of our interest are those carried in the blood, including plasma and white and red blood cells, the amount of which is proportional to the volume of the blood vessels:

$$V = \pi r^2 l. \tag{2}$$

In the cost function, the constant π is dropped so MC is solely defined by the radius and length of each vessel segment.
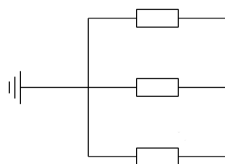
FIGURE 4. Power cost schematic diagram. The vessel branching is considered as a parallel circuit.

Next, we consider the power cost (PC), which represents the total energy dissipated in blood circulation. The power loss in a vessel is defined as:

$$P_{loss} = Q^2 R, \tag{3}$$

where Q is the flow rate and R is the resistance of the vessel. The flow rate Q indicates the amount of blood flowing through a single cross-section of the vessel per unit time:

$$Q = \frac{\Delta p}{R}, \tag{4}$$

where Δp is the pressure difference of the two vessel ends. A vessel segment, with a fluid flow described by the Hagen-Poiseuille equation, can be considered analogous to a resistor which follows Ohm's law, while the pressure difference Δp and flow rate Q are analogous to the voltage and current, respectively. We can then regard the root of each vessel tree as the ground of the circuit (Fig. 4).

Besides, the force needed to pump the blood in a vessel is:

$$\Delta F = \pi r^2 \Delta p = \frac{8\mu l Q}{r^2}, \tag{5}$$

where μ is the blood viscosity. The pressure difference is then

$$\Delta p = \frac{8\mu l Q}{\pi r^4}. \tag{6}$$

Combining (6) and (4), we have:

$$R = \frac{\Delta p}{Q} = \frac{8\mu l}{\pi r^4}. \tag{7}$$

Then we drop all constant terms and combine (3) and (7). The power cost thus depends only on the radius and length of the vessels. Note that the above equation represents the resistance of a single vessel segment.

Our assumptions lead us to model the vessels at a branching point as a parallel circuit to compute the total power cost of the blood inflow and outflows. The inlet vessel is the main circuit with the main resistance R_0 and the branching vessels are the branching circuits with resistance R_i, $i = 1, \ldots, n$. By Ohm's law, the equivalent resistance of all vessel outlets is:

$$\frac{1}{R_{out}} = \sum_{i=1}^{n} \frac{1}{R_i}. \tag{8}$$

We now derive the restrictions of the optimization problem. First, consider Murray's law [23]:

$$Q_{in} = Q_{out}, \tag{9}$$

$$r_0^c = \sum_{i=1}^{n} r_i^c, \tag{10}$$

where the coefficient c is set to 3 in correspondence to branchings in small arteries. In reality, c can range from 2 for large vessels to 3 for small ones [4]. Furthermore, according to [24], the vessel radius of major cerebral vessels generally ranges from 0.5 mm to 2.5 mm.

Combining (1) and (2) for MC and (3), (7) and (8) for PC, we can obtain the total cost function, which we will minimize over the length l and radius r of each vessel branch. Note that in the algorithm implementation, rather than directly specifying l and r for every vessel, we define the network structure by the locations of the bifurcation points and the three associated radii as in Fig. 1. Then, l's can be calculated as the distance between the bifurcation point and its neighbor nodes. The resulting optimization problem is:

$$
\begin{aligned}
\text{minimize } & C = MC + PC \\
& = \gamma \cdot \sum_{i=0}^{n} (2r_i l_i + r_i^2 l_i) + \frac{l_0}{r_0^4} + \frac{1}{\sum_{i=1}^{n} \frac{r_i^4}{l_i}}, \\
\text{subject to: } & \\
& 0.5 \ mm < r_i < 2.5 \ mm, \quad i > 0, \\
& r_0^3 = \sum_{i=1}^{n} r_i^3
\end{aligned}
\tag{11}
$$

where the weight parameter γ is chosen as a hyperparameter to make the material cost and the power cost have a balanced

(a) 3D brain angiography   (b) Segmented vessel mesh   (c) Extracted centerlines
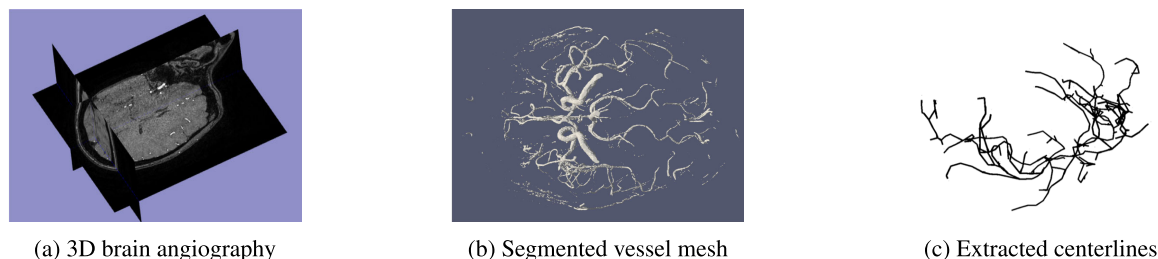
FIGURE 5. Patient-prior preprocessing before vascular network reconstruction. (a) The original brain angiography obtained from the IXI dataset. (b) We complete the cerebral artery segmentation with *vesseg*. (c) Vessel centerlines are extracted using *binvox* and *thinvox* sequentially. This centerline structure consists of locations and connection information for nodes along the segmented vessels. It is used as the input to our proposed GCO Forest algorithm.

effect on the cost function. In our experiments, we tried different γ's and studied the effects of material cost and power cost on the total cost function. From our results and the previous work done by Keelan *et al.* [25], we set γ to 642.

4) ALGORITHM FOR LOCAL OPTIMIZATION (RELAXATION)

Now, we discuss the specific algorithm used to find local optimal branching parameters given the cost function. We considered a variety of established optimization algorithms, including gradient descent, surrogate-based analysis, and simulated annealing, and examined their performance based on the network model complexity. The gradient descent method suffers from getting stuck in local optima and the surrogate-based method requires re-training of the surrogates at every step. In coping with multivariate optimization problems, the simulated annealing method is computationally more feasible because it is not affected by the initialization and avoids local optima by sampling a large portion of the parameter domain. Hence, we chose simulated annealing in implementing our framework.

The simulated annealing method is analogous to the annealing process in metallurgy [26]. In this method, a temperature parameter T with initial value T_0 decreases over iterations. In every iteration, the algorithm makes a set of moves, i.e., transformations in the parametric space, which may be accepted or rejected. The new state achieved after the move corresponds to a new value for each parameter in the domain and a new cost. Every good move, i.e., one that decreases the cost, is accepted whereas the bad moves are rejected with a certain probability. The probability of acceptance for a bad move depends on the temperature and is defined as:

$$\epsilon = \exp\left(-\frac{c_{new} - c_{old}}{T}\right), \tag{12}$$

where c_{new} is the value of cost function at the newly sampled point of the parameter space and c_{old} is the cost at the existing point. The threshold probability p_t is chosen by

$$p_t = Rand\left([0, 1]\right) \tag{13}$$

The value of ϵ is then compared with p_t. If $\epsilon > p_t$ the move is accepted, otherwise it is rejected.

In the beginning, when the temperature is high, the algorithm has a high probability of accepting moves. As the temperature falls, it prefers moves that significantly bring the cost down. At the end of the cooling cycle, the algorithm gets close to the global optimum. Its exploration of the entire parameter domain sets it apart from other optimization techniques and allows it to overcome local optima.
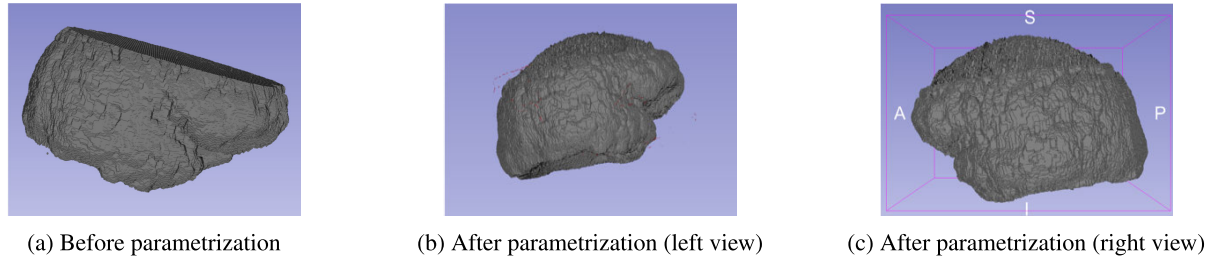
III. RESULTS

A. APPLICATION TO 3-D CEREBRAL ANGIOGRAPHY

Our proposed reconstruction framework involves many steps in addition to our patient-specific GCO Forest optimization algorithm detailed in Section II. The flowchart of the entire process involved in the framework is presented in Fig. 11 in the Appendix, where we summarize essential intermediate steps of the framework, including clinical image segmentation, root and leaf node selection, as well as GCO Forest optimization.

The proposed reconstruction framework theoretically can be applied to any organ. In this section, to show the performance of our proposed framework, we apply it to reconstruct patient-specific cerebral vascular network models from clinical image data collected in the brain of a patient. Before applying our proposed GCO Forest optimization method, we follow the flowchart of Fig. 11 (Appendix) and first preprocess the medical image and extract the patient's main vessel structure as well as the inner cortical volume.

1) DATA

Our dataset consists of brain MRA images of healthy subjects taken at Guy's Hospital, London (UK) using a Philips 1.5T scanner and released under Creative Commons License by the Imperial College London (IXI Dataset) [27]. The brain volume has size $512 \times 512 \times 100$ in pixels and spacial resolution 0.3125 mm $\times$ 0.3125 mm $\times$ 0.6 mm on the coronal, sagittal, and axial axes, respectively (Fig. 5a). The reconstruction framework is majorly implemented in python 3.5. During testing, five synthetic networks are generated inside the cortical volume with varying random seeds to study the algorithm dependency on initialization.

(a) Before parametrization   (b) After parametrization (left view)   (c) After parametrization (right view)

FIGURE 6. Brain volume completion by parameterization. (a) Sometimes, the patient prior can be incomplete, which makes our algorithm hard to apply. (b), (c) We use second-order polynomial to parameterize the brain shape. We can then apply our GCO Forest algorithm to the complete model.

2) IMAGE PREPROCESSING WITH INTENSITY PROJECTION

Prior to segmentation, we employ several preprocessing strategies mentioned in [28] to increase the contrast between vessels and adjacent tissues. First, the intensity range of the image is normalized to [0, 255] using

$$f(x) = \frac{x - min(X)}{max(X) - min(X)} \times 255, \qquad (14)$$

where X denotes the set of intensities for all pixels in an image. The intensity values are then clipped by a threshold value c, leaving

$$g(x) = \begin{cases} c, & x > c \\ x, & x <= c \end{cases} \qquad (15)$$

and normalized again by $f(x)$. Our experiments showed that $c = 200$ is optimal for the specific clinical image stack we used. In addition, we project the resulting intensities by the function $q(x) = x^p$. We tested quadratic and cubic projections, i.e., $p = 2$ and $p = 3$, as in [28] and chose the cubic projection in our reconstruction framework.

3) SEGMENTATION AND ROOT NODE SELECTION

Though the proposed reconstruction framework takes advantage of clinical images, the exact segmentation procedure is well-studied by a variety of works and is beyond the scope of this paper. We employ previously established algorithms to acquire the vascular information needed for network structure optimization. In particular, cerebral artery segmentation (Fig. 5b) is achieved using the python package *vesseg* [29], which takes advantage of *NiftyNet*, a 3-D convolutional neural network architecture designed specifically for clinical image processing. To represent the resulting mesh with a 3-D array, we use *binvox* [30], [31] on the segmented vessel model to rasterize it into a binary 3-D voxel grid and then apply a thinning algorithm *thinvox* [32], [33] to calculate the vessel centerlines. We then perform Connected Component Analysis [34] to keep only the main CoW vessels, discarding major discontinuities (Fig. 5c).

For our test dataset, we chose 1100 points from the segmented vessels as the root nodes and connected them together using the method presented in Section II-C. The number was selected practically to ensure the detailedness of the network while maintaining the computational cost manageable.

Thus, we can convert the vasculature information in the clinical image into a mathematical network model that satisfies the assumptions described in Section II-A.

4) BRAIN PARAMETERIZATION AND LEAF NODE SELECTION

Because the target area of the scans is sometimes specific parts of the patient's brain, in some cases, the angiographies at hand might not contain the entire brain volume (Fig. 6a). For example, the image stack in our dataset only contains the lower part of the brain, making it impossible to sample leaf nodes from the entire cortex area. We deal with this problem by parameterizing the upper part of the brain and complete the brain volume. For complete data that are ready to use, we can simply skip the parameterization process.

Prior to brain parameterization, we first extract the partial surface of the cerebral cortex with the software *BrainSuite*. Along the sagittal axis, we cut the volume into 500 coronal slices and fit the following curves to the existing points on the surface of the cerebral cortex in each coronal plane.

- Second-order polynomial:

$$y = ax^2 + bx + c \qquad (16)$$

- Circle:

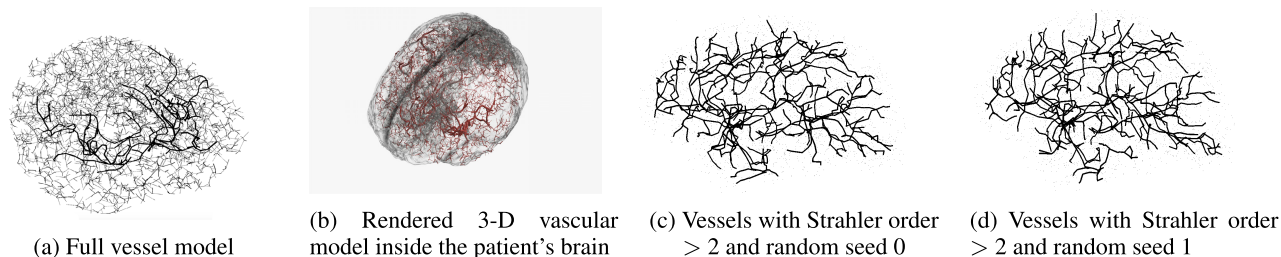$$\frac{x^2}{a^2} + \frac{y^2}{b^2} = 1 \qquad (17)$$

- Ellipse:

$$(x - a)^2 + (y - b)^2 = 1 \qquad (18)$$

Comparing the parameterization results, we found that the polynomial and ellipse curves gave more realistic cortical surfaces. For computational efficiency, we use polynomial parameterization in our framework (Fig. 6b and 6c).

After a second-order polynomial is fitted within each plane, we put the slices back together and fill up the cortical volume. The leaf selection algorithm (Section II-C2) is then applied to this volume. For our dataset, 3000 terminal nodes are sufficient to produce a detailed vascular network.

5) OPTIMIZATION

We used the algorithm described in Section II-D4 to minimize the cost function defined in Section II-D3 locally at each

(a) Full vessel model

(b) Rendered 3-D vascular model inside the patient's brain

(c) Vessels with Strahler order > 2 and random seed 0

(d) Vessels with Strahler order > 2 and random seed 1

FIGURE 7. Reconstructed vascular networks using the GCO Forest algorithm. (a) The network is generated with over 3000 leaf nodes. The thick edges denote the segmented main vessels from the image data. (b) Rendered 3-D model inside the patient's brain. (c) and (d) Two vessel models with Strahler order greater than 2 (right view). The models are independently generated with different random seeds, but exhibit similar overall structures.

node. To accomplish this, the algorithm searches for the optimal branching condition in the six-dimensional parametric space: the three spatial coordinates (x, y, z) of the bifurcation point and the radii of the three vessels meeting at that point (Fig. 1). The three coordinates may alternatively be considered as the lengths of the three vessels, as fixing one fixes the other. The simulated annealing algorithm starts from a random point in the parametric space and explores this space by making one move at a time. The move function has to be so chosen that it allows the algorithm to effectively scan the entire domain without moving too far from a potential optimum in a single move. In our framework, we set the step size to 0.5% of the target value's range. Thus, the move function is of the form

$$0.005 \times Rand([-1, 1]) \times (max(V) - min(V)), \quad (19)$$

where V is the variable to be optimized, i.e., the vessel radius or the bifurcation point coordinates. In one move, the algorithm moves independently along five of the six dimensions using the above move function. The sixth (r_0 or parent vessel radius) coordinate is calculated from the radii of the branches, after the move, using Murray's Law (Eq. 10).

Associated with every move is a change in the cost. For the three dimensions of vessel radii, there is an additional range constraint (The radii should not exceed the specified limits in Eq. 11). This is incorporated using the penalty formulation; every move that exceeds the limits incurs a penalty which adds to the cost. Hence, such moves are not likely to get accepted.

The acceptance probability of a new move depends on the cost and the temperature. Since the numerical order of the cost is problem-dependent, the temperature needs to be adjusted to make the probabilities feasible. In our problem setting, the starting temperature is set to 1 and cooling is done until it dropped to 0.001. This choice of temperature keeps the acceptance probabilities in check throughout the cooling cycle and allowed the achievement of the global optimum. The rate of cooling affects the algorithm's ability to settle at the right value. A small cooling coefficient may cause the algorithm to get stuck in a local optimum, whereas a large value combined with a big move function may prevent settling at a solution. In our framework, the cooling rate is set to 0.999. The customized simulated annealing algorithm

is implemented in C with a python wrapper to integrate it into our global constructive optimization framework.

At the end of the cooling cycle, the node position and the corresponding vessel radii reach their globally optimum values for the given configuration. Repeating this procedure for each node, combined with merging and splitting when required (See sec. II-D2), leads to optimization of the overall tree structure. However, this structure is still a derivative of the initial topology and inherits its global features. Therefore, the tree is pruned (up to the vessels of a specified order) and the nodes reconnected to the nearest neighbors, which modifies the network topology. The same optimization cycle is then repeated for this topology and the pruning threshold is decreased after every such iteration. This cycle ultimately leads to the globally optimized network as discussed in Section II-D2.

B. VALIDATION

To demonstrate the validity of our proposed vessel reconstruction framework, we compared the morphometric and physiological properties of our reconstructed network with cerebral vessel data collected in humans. We followed the flowchart in Fig. 11 and reconstructed a set of cerebral vascular networks from the patient dataset described in Section III-A1 using five random seeds. We sampled over 3000 leaf nodes and 1000 root nodes for optimization. An example reconstructed network is shown in Fig. 7a, and the rendered 3-D brain model is shown in Fig. 7b. In Fig. 7a, the thick branches correspond to the vessels segmented from the clinical image and the branches in gray are constructed by our GCO Forest algorithm.

1) MORPHOMETRIC ANALYSIS OF RECONSTRUCTED NETWORK

To validate the reconstructed network, we compared its morphometric properties with data collected in the human brain using confocal laser microscopy and 3-D computer-assisted methods [35], [36].

We first analyzed the frequency distributions of vessel diameters and lengths. In our models, a vessel segment is defined as the cylinder between two connected nodes. The diameter of a segment is optimized in GCO and converges to

TABLE 1. Statistics of length *L* and diameter *D* distributions of the generated main vascular network model. After applying the inverse square root and natural logarithm functions, the vessel diameter and branch length have similar mean and median, respectively. So the distributions are approximately normalized. The distance metrics show that with different random seeds, the generated network have similar characteristics in terms of vessel diameter and branch length distribution. Note that the unit for diameters is *mm*. Compared to the work of Lauwers *et al.*, our statistics only summarize the main vessels but not the capillaries, therefore the overall scale is slightly larger than the statistics of Lauwers *et al.*.

	Diam (mm)	$1/\sqrt{D}$	Length (mm)	$\log L$
Mean	1.51	0.86	9.77	1.99
Standard deviation	0.68	0.13	5.79	0.82
Median	1.37	0.85	8.09	2.03
Interquartile range	1.15/1.72	0.76/0.93	4.16/13.17	1.42/2.65
Skewness	3.64	0.06	1.08	-0.46
Kurtosis	20.52	2.66	13.12	3.90
Correlation	0.94	0.94	0.99	0.99
Chi-square distance	1.71	4.66	0.02	0.10
Bhattacharyya distance	0.14	0.13	0.04	0.03

(a) Distribution of D

(b) Distribution of $1/\sqrt{D}$

(c) Distribution of L
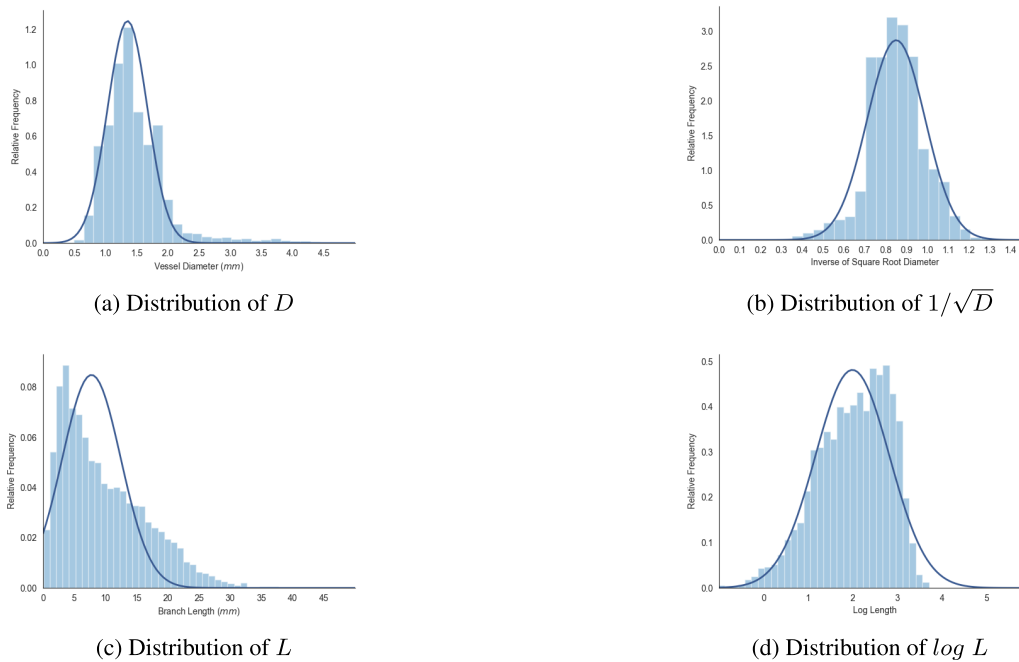

(d) Distribution of $\log L$

FIGURE 8. Characteristics of length *L* and diameter *D* of the reconstructed vascular network. (a) Distribution of *D* is right-skewed. (b) Distribution of *D* can be normalized by the inverse of square root function. (c) Distribution of *L* is right-skewed. (b) Distribution of *L* can be normalized by the natural logarithm function.

a local optimum under the predefined cost function. The segment length is calculated as the Euclidean distance between the two nodes. The distributions are shown in Fig. 8 and are averages of the individual histograms generated from the five random seeds. The statistics in Table 1 are also averaged across five random seeds. Consistent with the actual human brain data in [35], none of the distributions are normal. Rather, they are asymmetric with large positive skewness and kurtosis. However, as Fig. 8b and 8d show, the logarithm of the vessel length and the inverse of the square root of the diameter conform to normal distributions with means and medians close together. The skewness is close to 0 and kurtosis is close to 3. These characteristics agree with prescribed statistics in [35]. Note that the vessel diameters and lengths in our model is larger in scale compared with their statistics.

This is because our generated network consists of the main vasculatures and omits some capillaries segment, whereas Lauwers *et al.* [35] measured the complete cerebral network including the capillaries.

In addition, in the vascular network reconstructed by our proposed method, the log frequency, average diameter, and length of vessels follow a linear relationship with the Strahler order (Fig. 9). The plots are consistent with Figure 9c in [37] and indicate the fractal nature of the network.

Although the main network structure was obtained from the patient data, all branches underwent heavy remodeling in the course of optimization. Moreover, the vessel formation in our reconstruction process was inherently stochastic due to the simulated annealing algorithm. In Fig. 7c and 7d, we present two network structures viewed from the same

(a) Strahler order log frequency

(b) Diameter v.s. Strahler order

(c) Branch length v.s. Strahler order
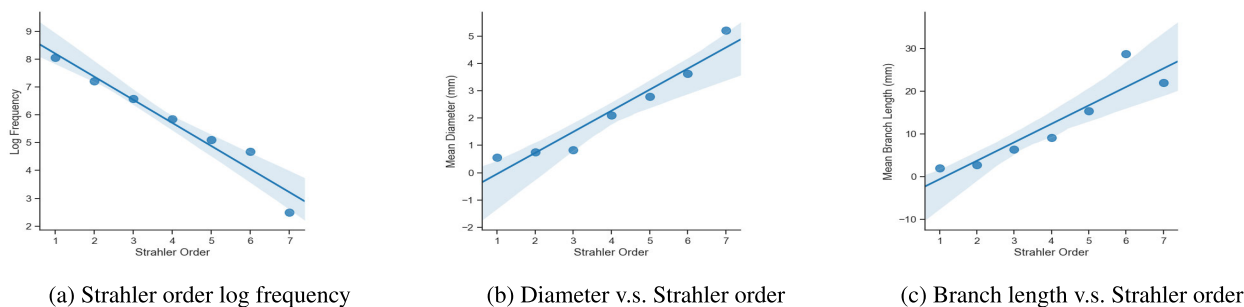
FIGURE 9. Strahler order and its relationship with vascular network characteristics. (a) The log frequency of Strahler order follows a linear function with a negative slope. The shaded area indicates the margin of error. (b) Vessel diameter is positively, linearly proportional to Strahler order. (c) Branch length is positively, linearly proportional to Strahler order. These characteristics indicate the fractal nature of the cerebral vascular network.

(a) Calculated pressure distribution in the vessels

(b) Shear stress induced in the vessel walls
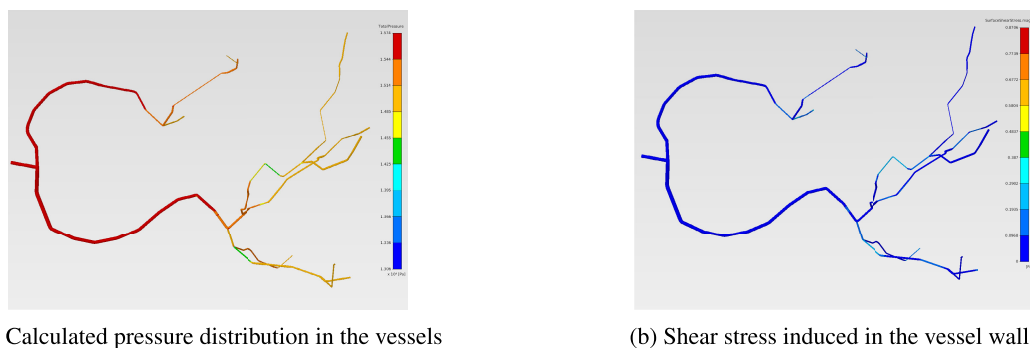
FIGURE 10. Flow simulation results. (a) The pressure within the network of higher-order cerebral arteries is found to vary smoothly from 15.74 kPa (118 mmHg) at the entry to about 15 kPa (112.5 mmHg) at exit, while falling to 13.06 kPa (98 mmHg) in the thinnest regions. (b) The wall shear stress in most regions of the network stays below 0.4 Pa with a maximum of 0.87 Pa, which lies in the normal range measured *in vivo* [38].

perspective with vessels whose Strahler orders are greater than 3. They were generated with different random seeds. The general branching patterns were analogous to each other, despite the small differences induced by varying moves taken in simulated annealing. We quantified the differences between the morphometry histograms of the two networks using three metrics: correlation, chi-square distance, and Bhattacharyya distance (Table 1). A strong correlation and small chi-square and Bhattacharyya distance scores imply that the histograms are similar to each other. In our experiments, all histograms display strong correlations and close-to-zero distance scores. This suggests that the stochastic nature of the GCO Forest algorithm is restrained by our carefully designed cost function and that our proposed patient-specific framework could reconstruct cerebral vessel networks that are morphometrically similar to the ones in the human brain.

2) HEMODYNAMIC ANALYSIS OF THE RECONSTRUCTED NETWORK

After analyzing the morphometry of the reconstructed vascular network, we further validated it by testing its physiological function. To this end, we studied the distribution of the internal blood pressure and the shear stress on the vessel walls using computational fluid dynamics. For the purpose of

this analysis, we only considered vessels with Strahler orders greater than 3, because a flow simulation of the entire network would be computationally expensive. The vessel walls were considered to be rigid and the physical boundary conditions were derived from available physiological data.

The inlet velocity was considered to be 50 cm/s and the blood pressure at the exit from the network was considered to be 112.5 mmHg [39]–[41]. We used the reported properties of blood at the normal body temperature (density: 1060 kg/m^3 and viscosity: 3 m·Pa/s). We obtained a steady-state solution using the implicit 'Coupled' scheme in *Fluent R16.0*. This scheme uses a pressure-based coupled solver, which simultaneously enforces continuity while solving for velocity using the momentum equation.

The calculated flow domain (Fig. 10) is physiological as the pressure varies smoothly along the network without abrupt changes and the wall shear stress is within the physiological range as measured by [38]. Thus, the reconstructed vascular network produces physiological hemodynamic behavior while morphometrically is similar to that of the human brain and respects the root and leaf relationships acquired from the patient prior. Moreover, for different random seeds, the geometrical and optimality constraints enforced by our algorithm lead to similar reconstructed vessel networks all of which successfully adapt to the patient

prior and correlate with the major segmented vessels of the patient's brain.

IV. DISCUSSION

In this section, we present some related works, the benefits and the limitations of our algorithm in comparison with those methods. We also illustrate future works that can be done to improve the framework's practicality.

The core algorithm of the optimization framework in this paper is based on the practical observation that the departure from optimality in the human vascular structures will cause disease [42]. That is, our reconstruction method generates vascular networks of the human brain under the optimality assumption that the network structures will minimize both the material loss and the blood circulation power loss. With the same assumption, two types of angiogenesis-based optimization models have been proposed previously: (1) the constrained constructive optimization (CCO) [2], and (2) global constructive optimization (GCO) [4]. While CCO finds an optimal tree by adding one branch at a time, GCO performs a multi-scale optimization to find an optimal tree for all leaf nodes simultaneously [43]. Our GCO Forest algorithm extended GCO to use clinical images of non-convex organs in individual patients and to optimize multiple vascular trees at the same time. In Section III, we demonstrate that by combining clinical data with our GCO Forest algorithm, the proposed framework is able to generate realistic vascular networks that exhibit morphometric and hemodynamic similarities to actual brain vasculatures.

Several recent works have also combined image-based segmentation and optimization-based reconstruction. Jaquet *et al.* [5] use heart CT images and extend the constrained constructive optimization (CCO) method to generate multiple, competing coronary trees from large epicardial arteries to arterioles. Their method can simulate network forests within non-convex territories and the resulted models satisfy literature morphometry. However, their optimization method and targeted organ are fundamentally different from ours. The CCO method performs a single tree angiogenesis simulation by minimizing the total tree volume [2]. It optimizes the objective locally by adding one branch to an existing vessel tree at a time. Apart from the volume-related material cost, our GCO Forest algorithm also considers the power cost, minimizing a more comprehensive target function. In addition, we perform optimization at both local and global scales.

Compared with generating vascular networks in the liver, heart, and eye [2]–[5], cerebral vasculature reconstruction receives less research attention due to the following reasons. First, the shape of the target organ should be regular and mostly convex to reduce the difficulty of optimization. For convex territories, techniques like CCO are able to solve the problem because the surface of the organ can be parameterized by relatively simple mathematical expressions. Second, there is a single blood-flow inlet (one main artery) and multiple outlets in organs like the liver. Thus, the vasculature can

be generated by a single tree with one root node, reducing the computational cost. The human brain, on the other hand, satisfies neither of the above conditions. Due to the complexity of the brain structures, especially the curved surface of the cortical white matter, cerebral arteries lie within an irregular volume that cannot be easily parameterized. More importantly, the dynamics of blood flow in the human brain are determined by a complex network of vessels with the Circle of Willis (CoW) forming the central part of this network [44]. Blood is supplied by two internal carotid arteries (ICAs) and also by two vertebral arteries (VAs), which branch and link to form the CoW. Thus, our proposed framework is an important step towards reconstructing vasculature within an irregular volume, accounting for multiple blood-flow inlets and the interactions between the arterial trees.

Upon finishing this paper, we are aware that Ii *et al.* [45] have worked on a similar setting to us independently. Their proposed multilevel region-confined (MRC) algorithm generates image-based vasculatures by addressing hierarchical pathways and pair-wise coupling of the arterial and venous systems in the human brain. Their reconstructed networks consist of both arteries and veins at different scales for each brain region. However, the MRC algorithm is a geometry-prioritized version of the CCO model. In generating new vascular segments around terminal points, it omits the structural optimization part of CCO to reduce computational cost by choosing the nearest neighbor. Moreover, it employs a combinatorial optimization approach and only chooses from four predetermined bifurcation patterns. In contrast, our method effectively explores the entire domain in selecting a bifurcation point with the simulated annealing algorithm. Our modified GCO algorithm obtains a globally optimized network after multiple cycles of edge pruning and reconnection. MRC, however, is prone to variability because of the fixation of randomly selected terminal points based on features of the existing network (which might not always be optimal). Furthermore, we have utilized a more thorough validation methodology comprising of both morphometric and physiological analysis.

Nonetheless, our proposed reconstruction framework can be improved in the following aspects. First, the current workflow utilizes the segmented vessels from clinical images as the basis of the GCO Forest algorithm. However, we only preserve the main CoW arteries, discarding the other information such as small and discontinuous vessel parts. In fact, these small segments provide useful and crucial information about the exact arterial structure and should guide the reconstruction of patient-specific vascular networks. Our experiments demonstrated that the resulting network depends largely on the detailedness of the patient prior. Therefore, to improve the accuracy of the reconstructed network and make full use of the patient data, we can incorporate the locations and geometric properties of the detached segments into our algorithm.

Second, the stochastic nature of the optimization algorithm can be relaxed to achieve more deterministic vascular models. During the relaxation stage in GCO, we seek a
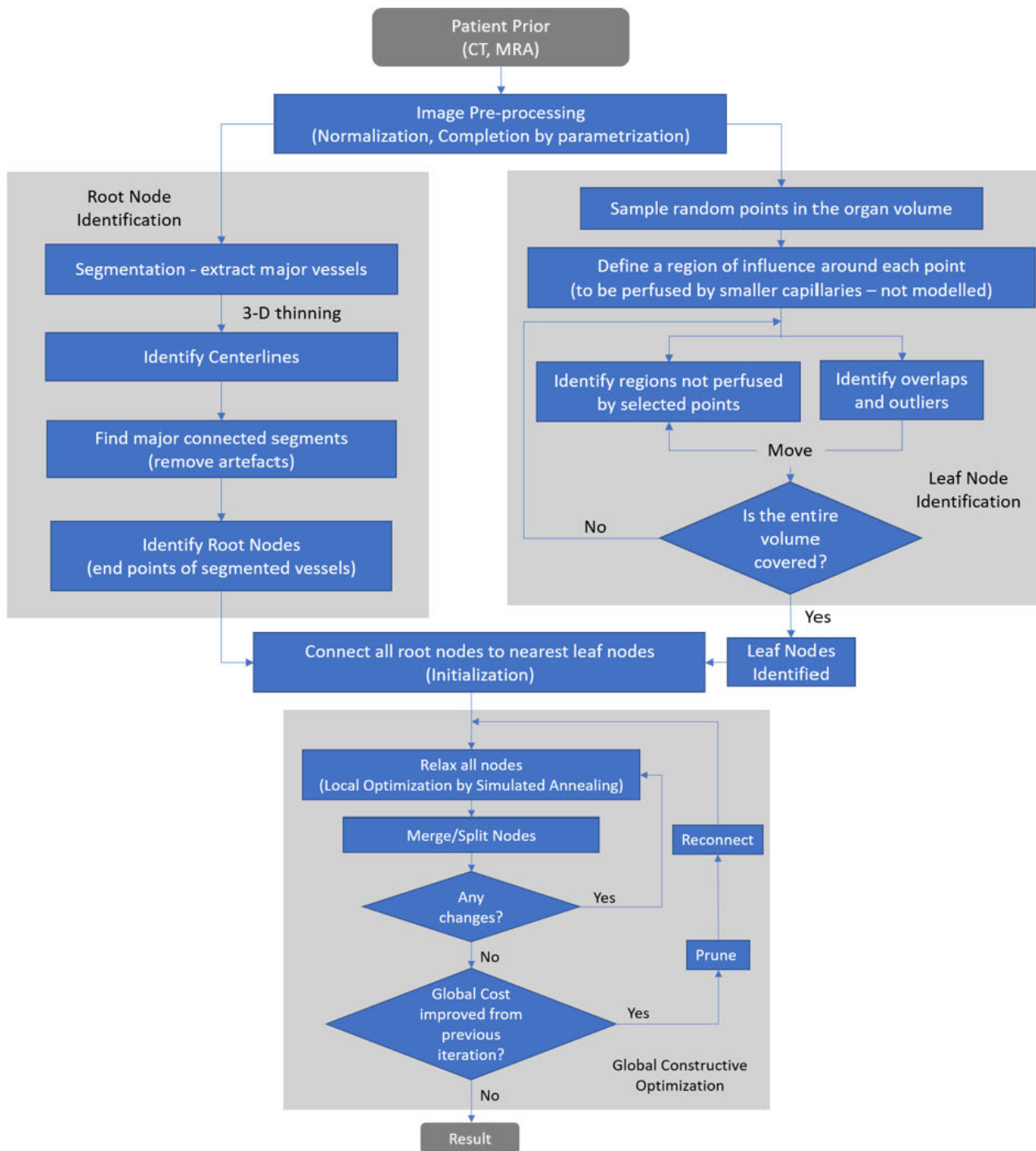
FIGURE 11. Flowchart of the complete computational framework. This flowchart summarizes the methodology discussed in Section III-A.

network configuration that minimizes the cost function. For each branching point, the x, y, z-coordinates of that point and the radii of the incident edges are all variables to be optimized. In the first few rounds of optimization, since there are not enough splittings, many leaf nodes are connected to one single intermediate node, resulting in an extremely complicated multivariate optimization problem with a non-convex

domain. Consequently, many optimization methods are inadequate to solve the problem. We thus turned to simulated annealing, where random moves are taken with a probability and the configuration with the minimum cost is recorded in the process. However, we are aware that the intrinsically stochastic nature of this optimization algorithm will lead to different models even with the same patient data. None of the

networks generated by our approach is an absolutely accurate reconstruction of the patient-specific cerebral vascular system. In future work, we can improve the robustness of our algorithm by combining several resulting networks together. In this way, we will search for an average model. Also, in future research, other promising optimization methods such as the nature-inspired method proposed in [46] or other recent algorithms [47]–[49] can be adopted to improve the optimal vascular network that our framework generates.

Moreover, though quantitative analysis reveals an impressing similarity in terms of scaling and branching properties between our reconstructed network and data gathered in the human brain, we have been unable to verify the network's gross vascular anatomy, branching patterns, and asymmetry directly. A potential approach for evaluation is to slightly change the segmented vessels in the initialization of GCO Forest, e.g., reducing the CoW vessel length, and quantify the differences between the final configurations. This would lead to an estimation of the robustness and predictive power of the reconstruction framework.

V. CONCLUSION

We developed a patient-specific framework for the reconstruction of vascular systems, which transforms raw image input into an augmented 3-D vascular model based on an extended global constructive optimization algorithm. The resulting network adapts to the brain shape and the major vessels segmented from clinical images of actual patients. To study the effect of randomness involved in the optimization process, we generated multiple cerebral vascular models from a single image stack and compared their differences. We further validated the reconstructed network structures by showing that the morphometric properties agree quantitatively with existing anatomical data of the human brain. Additionally, we used computational fluid dynamics to investigate the hemodynamic characteristics, such as the maximum wall shear stress, of the reconstructed networks. Blood flow simulation suggests that the numerical differences in the blood pressure and wall shear stress between our models and existing data are negligible and are not expected to have remarkable effects on cancer metastasis simulations that use the 3-D models reconstructed by our proposed method.

APPENDIX FLOWCHART
See Figure 11.

REFERENCES

[1] T. N. Seyfried and L. C. Huysentruyt, "On the origin of cancer metastasis," *Crit. Rev. Oncogenesis*, vol. 18, nos. 1–2, pp. 43–73, 2013.

[2] R. Karch, F. Neumann, M. Neumann, and W. Schreiner, "A three-dimensional model for arterial tree representation, generated by constrained constructive optimization," *Comput. Biol. Med.*, vol. 29, no. 1, pp. 19–38, Jan. 1999.

[3] W. Schreiner, R. Karch, M. Neumann, F. Neumann, P. Szawlowski, and S. Roedler, "Optimized arterial trees supplying hollow organs," *Med. Eng. Phys.*, vol. 28, no. 5, pp. 416–429, Jun. 2006.

[4] M. Georg, T. Preusser, and H. K. Hahn, "Global constructive optimization of vascular systems," Dept. Comput. Sci. Eng., Washington Univ. St. Louis, St. Louis, MO, USA, Tech. Rep. Wucse-2010-11, 2010. [Online]. Available: https://openscholarship.wustl.edu/cse_research/362

[5] C. Jaquet, L. Najman, H. Talbot, L. Grady, M. Schaap, B. Spain, H. J. Kim, I. Vignon-Clementel, and C. A. Taylor, "Generation of patient-specific cardiac vascular networks: A hybrid image-based and synthetic geometric model," *IEEE Trans. Biomed. Eng.*, vol. 66, no. 4, pp. 946–955, Apr. 2019.

[6] D. Szczerba and G. Székely, "Macroscopic modeling of vascular systems," in *Medical Image Computing and Computer-Assisted Intervention*, T. Dohi and R. Kikinis, Eds. Berlin, Germany: Springer, 2002, pp. 284–292.

[7] M. Kretowski, Y. Rolland, J. Bezy-Wendling, and J. Coatrieux, "Physiologically based modeling of 3-D vascular networks and CT scan angiography," *IEEE Trans. Med. Imag.*, vol. 22, no. 2, pp. 248–257, Feb. 2003.

[8] J. Brown, G. West, and B. Enquist, *Scaling Biology: Patterns Processes, Causes Consequences*. Oxford, U.K.: Oxford Univ. Press, Jan. 2000, pp. 146–147.

[9] T. J. Huppert, M. S. Allen, H. Benav, P. B. Jones, and D. A. Boas, "A multicompartment vascular model for inferring baseline and functional changes in cerebral oxygen metabolism and arterial dilation," *J. Cerebral Blood Flow Metabolism*, vol. 27, no. 6, pp. 1262–1279, Jun. 2007.

[10] T. R. Nelson and D. K. Manchester, "Modeling of lung morphogenesis using fractal geometries," *IEEE Trans. Med. Imag.*, vol. 7, no. 4, pp. 321–327, Dec. 1988.

[11] C. Y. Wang and J. B. Bassingthwaighte, "Area-filling distributive network model," *Math. Comput. Model.*, vol. 13, no. 10, pp. 27–33, 1990.

[12] H. K. Hahn, C. J. G. Evertsz, H.-O. Peitgen, and J. H. D. Fasel, "Fractal properties, segment anatomy, and interdependence of the human portal vein and the hepatic vein in 3D," *Fractals*, vol. 11, no. 01, pp. 53–62, Mar. 2003.

[13] C. Kirbas and F. Quek, "A review of vessel extraction techniques and algorithms," *ACM Comput. Surv.*, vol. 36, no. 2, pp. 81–121, Jun. 2004.

[14] A. Christodoulidis, T. Hurtut, H. B. Tahar, and F. Cheriet, "A multi-scale tensor voting approach for small retinal vessel segmentation in high resolution fundus images," *Comput. Med. Imag. Graph.*, vol. 52, pp. 28–43, Sep. 2016.

[15] U. T. V. Nguyen, A. Bhuiyan, L. A. F. Park, and K. Ramamohanarao, "An effective retinal blood vessel segmentation method using multi-scale line detection," *Pattern Recognit.*, vol. 46, no. 3, pp. 703–715, Mar. 2013.

[16] F. Caliva, A. Hunter, P. Chudzik, G. Ometto, L. Antiga, and B. Al-Diri, "A fluid-dynamic based approach to reconnect the retinal vessels in fundus photography," in *Proc. 39th Annu. Int. Conf. IEEE Eng. Med. Biol. Soc. (EMBC)*, Seogwipo, South Korea, Jul. 2017, pp. 360–364.

[17] E. Tekin, D. Hunt, M. G. Newberry, and V. M. Savage, "Do vascular networks branch optimally or randomly across spatial scales?" *PLOS Comput. Biol.*, vol. 12, no. 11, Nov. 2016, Art. no. e1005223.

[18] E. P. W. Helps and D. A. McDonald, "Observations on laminar flow in veins," *J. Physiol.*, vol. 124, no. 3, pp. 631–639, Jun. 1954.

[19] W. R. Gutierrez, "The optimal form of distribution networks applied to the kidney and lung," *J. Biol. Syst.*, vol. 15, no. 04, pp. 419–434, Dec. 2007.

[20] D. M. Moody, M. A. Bell, and V. R. Challa, "Features of the cerebral vascular pattern that predict vulnerability to perfusion or oxygenation deficiency: An anatomic study," *Amer. J. Neuroradiol.*, vol. 11, no. 3, pp. 431–439, 1990.

[21] A. F. Smith, V. Doyeux, M. Berg, M. Peyrounette, M. Haft-Javaherian, A.-E. Larue, J. H. Slater, F. Lauwers, P. Blinder, P. Tsai, D. Kleinfeld, C. B. Schaffer, N. Nishimura, Y. Davit, and S. Lorthois, "Brain capillary networks across species: A few simple organizational requirements are sufficient to reproduce both structure and function," *Frontiers Physiol.*, vol. 10, p. 233, Mar. 2019.

[22] J. Reichold, M. Stampanoni, A. L. Keller, A. Buck, P. Jenny, and B. Weber, "Vascular graph model to simulate the cerebral blood flow in realistic vascular networks," *J. Cerebral Blood Flow Metabolism*, vol. 29, no. 8, pp. 1429–1443, Aug. 2009.

[23] C. D. Murray, "The physiological principle of minimum work," *Proc. Nat. Acad. Sci. USA*, vol. 12, no. 3, pp. 207–214, 1926.

[24] P. Mouches and N. D. Forkert, "A statistical atlas of cerebral arteries generated using multi-center MRA datasets from healthy subjects," *Sci. Data*, vol. 6, no. 1, Dec. 2019, Art. no. 29.

[25] J. Keelan, E. M. L. Chung, and J. P. Hague, "Simulated annealing approach to vascular structure with application to the coronary arteries," *Roy. Soc. Open Sci.*, vol. 3, no. 2, Feb. 2016, Art. no. 150431.

[26] C.-R. Hwang, "Simulated annealing: Theory and applications," *Acta Appl. Math.*, vol. 12, no. 1, pp. 108–111, 1988.

[27] *Ixi Dataset*, I. C. L. Biomedical Image Analysis Group, Imperial College London, London, U.K., 2007.

[28] G. Tetteh, V. Efremov, N. D. Forkert, M. Schneider, J. Kirschke, B. Weber, C. Zimmer, M. Piraud, and B. H. Menze, "DeepVesselNet: Vessel segmentation, centerline prediction, and bifurcation detection in 3-D angiographic volumes," 2018, *arXiv:1803.09340*. [Online]. Available: https://arxiv.org/abs/1803.09340

[29] E. Gibson, W. Li, C. Sudre, L. Fidon, D. I. Shakir, G. Wang, Z. Eaton-Rosen, R. Gray, T. Doel, Y. Hu, T. Whyntie, P. Nachev, M. Modat, D. C. Barratt, S. Ourselin, M. J. Cardoso, and T. Vercauteren, "NiftyNet: A deep-learning platform for medical imaging," *Comput. Methods Programs Biomed.*, vol. 158, pp. 113–122, May 2018.

[30] F. S. Nooruddin and G. Turk, "Simplification and repair of polygonal models using volumetric techniques," *IEEE Trans. Vis. Comput. Graphics*, vol. 9, no. 2, pp. 191–205, Apr. 2003.

[31] P. Min. (2019). *Binvox*. [Online]. Available: http://www.patrickmin.com/binvox

[32] K. Palágyi and A. Kuba, "Directional 3d thinning using 8 subiterations," in *Discrete Geometry for Comput. Imag.*, G. Bertrand, M. Couprie, and L. Perroton, Eds. Berlin, Germany: Springer, 1999, pp. 325–336.

[33] P. Min. (2019). *Thinvox*. [Online]. Available: http://www.google.com/search?q=thinvox

[34] L. He, X. Ren, Q. Gao, X. Zhao, B. Yao, and Y. Chao, "The connected-component labeling problem: A review of state-of-the-art algorithms," *Pattern Recognit.*, vol. 70, pp. 25–43, Oct. 2017.

[35] F. Lauwers, F. Cassot, V. Lauwers-Cances, P. Puwanarajah, and H. Duvernoy, "Morphometry of the human cerebral cortex microcirculation: General characteristics and space-related profiles," *NeuroImage*, vol. 39, no. 3, pp. 936–948, Feb. 2008.

[36] F. Cassot, F. Lauwers, C. Fouard, S. Prohaska, and V. Lauwers-Cances, "A novel three-dimensional computer-assisted method for a quantitative study of microvascular networks of the human cerebral cortex," *Microcirculation*, vol. 13, no. 1, pp. 1–18, Jan. 2006.

[37] M. Schneider, J. Reichold, B. Weber, G. Székely, and S. Hirsch, "Tissue metabolism driven arterial tree generation," *Med. Image Anal.*, vol. 16, no. 7, pp. 1397–1414, Oct. 2012.

[38] R. S. Reneman and A. P. G. Hoeks, "Wall shear stress as measured *in vivo*: Consequences for the design of the arterial system," *Med. Biol. Eng. Comput.*, vol. 46, no. 5, pp. 499–507, May 2008.

[39] W. M. Blackshear, D. J. Phillips, P. M. Chikos, J. D. Harley, B. L. Thiele, and D. E. Strandness, "Carotid artery velocity patterns in normal and stenotic vessels.," *Stroke*, vol. 11, no. 1, pp. 67–71, Jan. 1980.

[40] P. Blanco, L. Mueller, and J. D. Spence, "Blood pressure gradients in cerebral arteries: A clue to pathogenesis of cerebral small vessel disease," *BMJ—Stroke Vascular Neurol.*, vol. 2, pp. 2017, Jun. 2017.

[41] W. A. Kofke, P. Brauer, R. Policare, S. Penthany, D. Barker, and J. Horton, "Middle cerebral artery blood flow velocity and stable xenon-enhanced computed tomographic blood flow during balloon test occlusion of the internal carotid artery," *Stroke*, vol. 26, no. 9, pp. 1603–1606, Sep. 1995.

[42] K. R. Hoffmann, "Automated three-dimensional vascular reproduction from stereoangiograms," in *Proc. Annu. Int. Conf.*, vol. 1, Nov. 1988, pp. 406–407.

[43] L. O. Schwen and T. Preusser, "Analysis and algorithmic generation of hepatic vascular systems," *Int. J. Hepatol.*, vol. 2012, pp. 1–17, Dec. 2012.

[44] D. Purves, G. Augustine, and D. Fitzpatrick, "The blood supply of the brain and spinal cord," in *Neuroscience*. 2nd ed. Sunderland, MA, USA: Sinauer Associates, 2001. [Online]. Available: https://www.ncbi.nlm.nih.gov/books/NBK11042/

[45] S. Ii, H. Kitade, S. Ishida, Y. Imai, Y. Watanabe, and S. Wada, "Multiscale modeling of human cerebrovasculature: A hybrid approach using image-based geometry and a mathematical algorithm," *PLOS Comput. Biol.*, vol. 16, no. 6, pp. 1–28, 06 2020.

[46] H. Zapata, N. Perozo, W. Angulo, and J. Contreras, "A hybrid swarm algorithm for collective construction of 3D structures," *Int. J. Artif. Intell.*, vol. 18, no. 1, pp. 1–18, 2020.

[47] R.-E. Precup, R.-C. David, E. M. Petriu, A.-I. Szedlak-Stinean, and C.-A. Bojan-Dragos, "Grey wolf optimizer-based approach to the tuning of pi-fuzzy controllers with a reduced process parametric sensitivity," *IFAC-Papers Line*, vol. 49, no. 5, pp. 55–60, 2016.

[48] A. Soares, R. Rábelo, and A. Delbem, "Optimization based on phylogram analysis," *Expert Syst. Appl.*, vol. 78, pp. 32–50, Jul. 2017.

[49] R.-E. Precup and R.-C. David, *Nature-Inspired Optimization Algorithms for Fuzzy Controlled Servo Systems*. Oxford, U.K.: Butterworth-Heinemann, 2019. [Online]. Available: https://www.sciencedirect.com/book/9780128163580/nature-inspired-optimi%zation-algorithms-for-fuzzy-controlled-servo-systems

JUNHONG SHEN was born in Beijing, China, in 1999. She is currently pursuing the B.S. degree in mathematics of computation with the University of California at Los Angeles.

From 2019 to 2020, she was a Research Assistant with the Center for Vision, Cognition, Learning, and Autonomy (VCLA). Her work focuses on reinforcement learning and control, communicative learning, and optimization. She is broadly interested in how machine can acquire greater learning ability with insights from human cognitive and communicative skills. In Summer 2019, she joined the Fields Undergraduate Research Program and worked as a member of the Computational Metastasis Laboratory, Department of Systems Design Engineering, University of Waterloo, where she studied vascular network reconstruction and optimization algorithms.
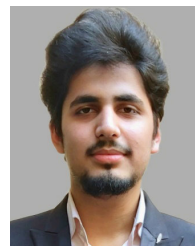
ABDUL HANNAN FARUQI was born in Aligarh, India, in 1998. He graduated from Our Lady of Fatima High School, Aligarh, with recognition of "Excellence in Academics." He received the B.Tech. degree (Hons.) in mechanical engineering from Aligarh Muslim University, Aligarh, in 2020. He is currently pursuing the M.S. degree in mechanical engineering, with a specialization in robotics and automation, with the Indian Institute of Technology Kanpur (IIT-K), India.

From 2018 to 2020, he performed his undergraduate research at the Computational Aerodynamics Laboratory, Aligarh Muslim University, and developed advanced algorithms for flow simulation and stability analysis. In Summer 2019, he participated in the Fields Undergraduate Summer Research Program at The Fields Institute, Toronto, Canada, where he undertook the study presented herein. He is currently a Graduate Research Assistant in Robotics at IIT-Kanpur. His research interests include the areas of computational algorithms, autonomous systems, and fluid dynamics. He seeks to develop advanced real-time computational techniques for integrating cognitive abilities in autonomous systems. He has written a chapter for *Modern Mathematical Methods and High Performance Computing in Science and Technology* (Springer, 2020).

Mr. Faruqi was a recipient of the Post Graduate Scholarship at IIT-K, the J. Brammer Graduate Research Fellowship, the Sir Syed Global Scholar Award, and the National Standard Examination-Certificate of Merit in Biology, in 2016. His team was the National Winner in Smart India Hackathon–2019, organized by Government of India.
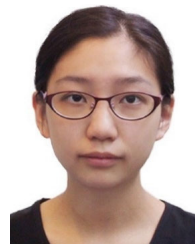
YIFAN JIANG received the bachelor's degree in mathematics and statistics from the University of Toronto, Canada, in 2020. She is currently pursuing the Ph.D. degree with The Pennsylvania State University, USA. Her research interests include variable selection for high-dimensional data and semiparametric regression modeling.

NIMA MAFTOON received the B.S. degree in mechanical engineering from the Isfahan University of Technology, the M.S. degree in mechanical engineering from the University of Tehran, and the Ph.D. degree in biomedical engineering from McGill University, in 2014. Then, he held a postdoctoral training at the Harvard Medical School, where he became a Junior Faculty Member, in 2016. He is currently an Assistant Professor with the University of Waterloo, where his research is dedicated to diagnostic and therapeutic solutions for cancer and hearing loss.

● ● ●